Film-Stabilizing Attributes of Polymeric Core–Shell Nanoparticles

Xiao-Jing Cai,[†] Hao-Miao Yuan,[†,⊥] Anton Blencowe,[‡,§] Greg G. Qiao,[‡] Jan Genzer,[*,†] and Richard J. Spontak[*,†,∥]

[†]Department of Chemical & Biomolecular Engineering, North Carolina State University, Raleigh, North Carolina 27695-7905, United States, [‡]Department of Chemical & Biomolecular Engineering, University of Melbourne, Parkville, Victoria 3010, Australia, [§]Mawson Institute, Division of ITEE, The University of South Australia, Mawson Lakes, South Australia 5095, Australia, and [∥]Department of Materials Science & Engineering, North Carolina State University, Raleigh, North Carolina 27695-7907, United States. [⊥]Present address: Department of Polymer Science & Engineering, University of Massachusetts, Amherst, MA 01003.

ABSTRACT Self-organization of nanoparticles into stable, molecularly thin films provides an insightful paradigm for manipulating the manner in which materials interact at nanoscale dimensions to generate unique material assemblies at macroscopic length scales. While prior studies in this vein have focused largely on examining the performance of inorganic or organic/inorganic hybrid nanoparticles (NPs), the present work examines the stabilizing attributes of fully organic core–shell microgel (CSMG) NPs composed of a cross-linked poly(ethylene glycol dimethacrylate) (PEGDMA) core and a shell of densely grafted, but relatively short-chain, polystyrene (PS) arms. Although PS homopolymer thin films measuring from a few to many nanometers in thickness, depending on the molecular weight, typically dewet rapidly from silica supports at elevated temperatures, spin-coated CSMG NP films measuring as thin as 10 nm remain stable under identical conditions for at least 72 h. Through the use of self-assembled monolayers (SAMs) to alter the surface of a flat silica-based support, we demonstrate that such stabilization is not attributable to hydrogen bonding between the acrylic core and silica. We also document that thin NP films consisting of three or less layers (10 nm) and deposited onto SAMs can be fully dissolved even after extensive thermal treatment, whereas slightly thicker films (40 nm) on Si wafer become only partially soluble during solvent rinsing with and without sonication. Taken together, these observations indicate that the present CSMG NP films are stabilized primarily by multidirectional penetration of relatively short, unentangled NP arms caused by NP layering, rather than by chain entanglement as in linear homopolymer thin films. This nanoscale "velcro"-like mechanism permits such NP films, unlike their homopolymer counterparts of comparable chain length and thickness, to remain intact as stable, free-floating sheets on water, and thus provides a viable alternative to ultrathin organic coating strategies.

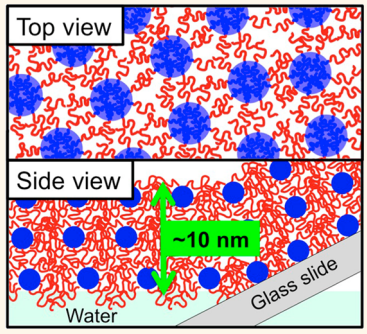

KEYWORDS: microgel particles · polymer thin film · nanolaminate · film stabilization · polymer coating · dewetting

A fundamentally interesting and technologically enticing aspect of contemporary nanoscience is the development of novel structures that form due to nanoparticle (NP) self-assembly, span multiple length scales and exhibit unique macroscopic properties. Glotzer, Kotov and co-workers[1–5] are indisputable pioneers in this field by repeatedly demonstrating that inorganic nanoscale colloids can be used to construct macroscale wires, ribbons and sheets, as well as a variety of unique assemblies, by understanding and applying the coupled effects of surface interactions (which can be altered through the addition of stabilizers), composition and shape. Of particular interest here are their free-floating NP sheets,[2,3] which constitute examples of extended assemblies by mimicking surface-layer proteins. In their study of amino-stabilized CdTe NPs measuring 3.4 nm in diameter, the driving force promoting monolayer formation *via* self-assembly relies mainly on a combination of different interactions, such as a dipole moment and hydrophobic attraction.[2] We return to this exciting observation later in the context of synthetically derived organic NPs. Unlike their inorganic counterparts, organic NPs consist primarily of polymeric building blocks and are therefore larger, broadly ranging from 10 nm to 1 μm across. Because they contain molecular chains that remain semiflexible at these dimensions,[6] such organic NPs can be effectively designed as nanospheres or nanocapsules. Polymeric nanospheres possess a

* Address correspondence to Jan_Genzer@ncsu.edu, Rich_Spontak@ncsu.edu.

Received for review January 12, 2015 and accepted July 4, 2015.

Published online July 04, 2015
10.1021/acsnano.5b00237

solid matrix, in which case their properties are chiefly regulated through surface modification.[7−10] Alternatively, nanocapsules contain an empty, yet potentially fillable, core that is surrounded by a solid organic shell.[11−13]

In general, polymeric NPs are prepared by either physical or chemical means and play increasingly important roles in, for example, sensory,[14] electronic,[15] photonic,[16] medical,[17,18] and environmental[19,20] applications. Physical methods frequently used to generate preformed polymeric NPs[21] include solvent evaporation,[22] salting-out,[23] precipitation,[24] dialysis[25] and supercritical fluid deposition.[26] The chemical route by which to produce such NPs employs various synthetic approaches, such as emulsion (including mini- and micro-),[27−29] interfacial[30] and controlled/living radical polymerizations.[31,32] This strategy can also be used to generate hybrid NPs possessing an inorganic core and an organic shell[33−36] or, of more direct relevance to the present study, microgel NPs wherein the chains are chemically cross-linked and, depending on the chemical constitution, responsive to external stimuli (*e.g.*, temperature, pH, salt, or applied electric field).[37−44] These hybrid and microgel NP designs can be combined to yield fully organic core−shell microgel (CSMG) NPs (also designated[45] as "core cross-linked star polymers") with a chemically cross-linked A core and surface-grafted B chains often referred[46,47] to as "arms", which can interact freely with their environment. While Wooley and co-workers[48−51] have established that the reverse arrangement (*i.e.*, shell cross-linked NPs) can likewise be of tremendous interest and practical use, we only consider the CSMG NP design further. More specifically, the CSMG NP investigated here has been synthesized *via* the "arm-first" route by atom transfer radical polymerization (ATRP)[45,52] and previously introduced in a study of autophobicity-driven surface segregation in polymer nanolaminates.[53]

Prior endeavors aimed at utilizing CSMG NPs to stabilize molecularly thin polymer films have relied exclusively on dispersing the NPs into a polymer thin film before the molten film destabilizes at elevated temperatures. For stabilization to occur in this scenario, the NPs must diffuse through the polymer matrix to a polymer interface, where they can alter the viscosity and/or chemical compatibility. Examples of nanoscale additives that have been reported to serve this function include fullerenes[54−56] and gold nanoparticles,[57,58] as well as latex nanoparticles[59] and dendrimers.[60] Failure to achieve satisfactory thin-film stabilization can be attributed to an insufficient number of arms on the CSMG[61] or mismatch between film destabilization and NP diffusion time scales. To explore the latter possibility, we have investigated the stability of nanoscale films composed entirely of CSMG NPs (*i.e.*, they are not dispersed in a homopolymer matrix) and surprisingly discovered several unique features, reported herein.

RESULTS AND DISCUSSION

The PEGDMA-PS CSMG NPs examined here were prepared *via* the arm-first approach and ATRP using a PS macroinitiator. The weight-average molecular weight ($\bar{M}_w$) of the CSMG NPs is 438 kDa and their gyration diameter in tetrahydrofuran (THF) is 29 nm, as determined by size exclusion chromatography equipped with multiangle laser light scattering (SEC-MALLS). Independent atomic force microscopy (AFM) analysis[62] of these NPs individually deposited onto Si wafer reveals that the cross-linked core is less than 3 nm in diameter, in favorable agreement with previous studies[63] of chemically similar CSMG NPs. The graft density of PS arms (σ_{PS}) is subsequently determined by dividing the number of arms per NP (32) by the surface area of the core, yielding a value of 1.13 arms/nm^2 on the basis of a 3 nm core diameter. A smaller core would produce a correspondingly larger value of σ_{PS}. Since $\sigma_{PS} > 1$, we presume that the arms are sufficiently packed to form a polymer brush.[64] This result, coupled with the relatively low molecular weight of the PS arms ($\bar{M}_w$ = 10.7 kDa), must be borne in mind during the following comparison with the linear PS homopolymer analog. Thin films composed of low-molecular-weight homopolymers become unstable and typically dewet from a solid substrate at temperatures above the glass transition temperature (T_g).[65] The illustrations displayed in Figure 1 depict films with a thickness of 40 nm spin-coated onto silica: linear PS homopolymer (Figure 1a) and the CSMG NP (Figure 1b). The molecular weight of the PS homopolymer (13.5 kDa) is similar to that of the PS arms on the NPs and is below the critical molecular weight of entanglement for PS ($M_{e,PS} \approx$ 18 kDa, according to Ferry[66]). As evidenced by the optical image in Figure 1c, the PS homopolymer film clearly dewets *via* nucleation and growth (NG) after only 2 min of annealing at 180 °C. The holes apparent in this image enlarge with time at a dewetting rate of 21 μm/min and ultimately impinge.

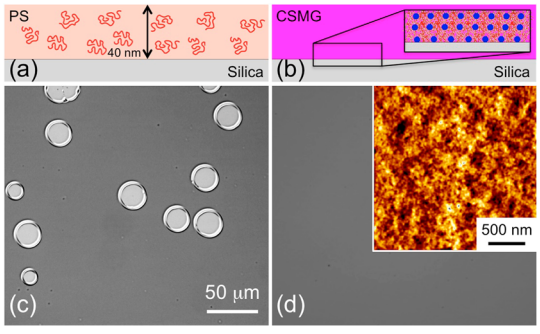

Figure 1. Schematic depictions of (a) PS and (b) CSMG NP thin films (thickness: 40 nm) spin-coated onto Si wafer. The molecular weight of the PS homopolymer (13.5 kDa) is comparable to that of the PS arms on the NPs (10.7 kDa). Optical images acquired from the corresponding thin films annealed at 180 °C are displayed for (c) 2 min and (d) 72 h. An AFM height image is included for the annealed CSMG NP thin film in (d).

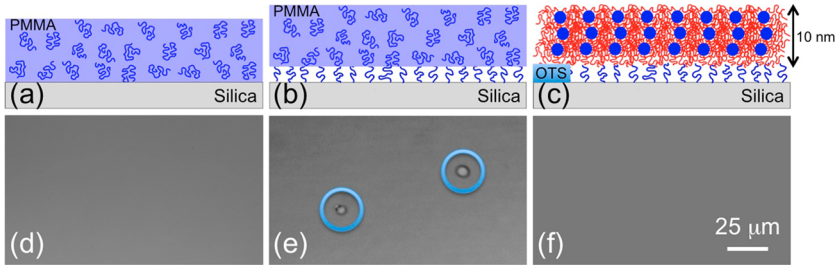

Figure 2. Illustrations of (a) a PMMA thin film spin-coated onto Si wafer, (b) a PMMA thin film floated onto an OTS SAM and (c) a CSMG NP thin film floated onto an OTS SAM. The molecular weight of the PMMA homopolymer (112 kDa) is comparable to that of the PEGDMA core of each NP (96 kDa). In all cases, the film thickness is 10 nm, and each SAM extends 1.2 nm from the surface of the silica layer located on top of a Si wafer. Optical images collected from the corresponding thin films annealed at 180 °C are displayed for (d) 72 h, (e) 15 min, and (f) 72 h.

In sharp contrast, the thin film composed of CSMG NPs remains stable under identical conditions even after 72 h at 180 °C (*cf.* Figure 1d). The AFM image included in the inset of Figure 1d further demonstrates that the film topography remains featureless even at nanoscopic length scales. Values of the root-mean-square (rms) roughness measured from the film surface before and after heat treatment are 0.94 and 0.49 nm, respectively, thereby confirming that such NP-based thin films are not affected by temperature in the same fashion as PS homopolymer thin films. In general, the stability of thin polymer coatings can be improved by increasing (i) the time scale associated with polymer chain mobility, (ii) the distance through which a rupture proceeds, and (iii) the physicochemical affinity between the coating and substrate. The first approach is achieved readily by increasing the polymer molecular weight, which promotes a corresponding increase in melt viscosity.[67] In this spirit, we have also examined two grades of PS homopolymer with molecular weights above (900 kDa) and below (216 kDa) the total molecular weight of the CSMG NPs (438 kDa). As anticipated, exposure of these high-molecular-weight PS films, spin-coated to a thickness of 10 nm on silica, to the same annealing conditions used to generate Figure 1d reveals that they do not display evidence of dewetting (*cf.* the Supporting Information) and are therefore deemed stable. The second strategy relates to the coating thickness, since a reduction in film thickness promotes a marked increase in dewetting rate (and possibly a transition to a different dewetting mechanism).[65,68,69] We explore the importance of this design consideration in a later section. Lastly, the affinity between the coating and substrate can be a system-specific consideration or it can alternatively be engineered through the use of surface templating.[70,71] In the present case, the rapid dewetting observed in Figure 1c indicates that low-molecular-weight PS possesses little affinity for silica. The CSMG NPs, however, consists of another chemical constituent, a cross-linked PEGDMA core, and the carbonyl group in acrylic polymers such as poly(methyl methacrylate) (PMMA) is known to undergo strong hydrogen bonding with the surface-bound hydroxyl groups on silica.[72]

To discern if the PEGDMA core in the NPs is capable of interacting with the silica substrate through the PS arms and therefore responsible for the enhanced film stability demonstrated in Figure 1d, we compare the stability of PMMA and CSMG NP films, each with a thickness of 10 nm, at 180 °C. Deposition of PMMA directly onto silica (illustrated in Figure 2a) results in a featureless, stable film even after 72 h of annealing (*cf.* Figure 2d), thus verifying the expectation that hydrogen bonding between PMMA and the silica substrate serves to stabilize the thin films.[72] The screening distance afforded by the existence of PS arms on the CSMG NPs is emulated here by modifying the silica surface with an *n*-octyltrichlorosilane (OTS) self-assembled monolayer (SAM) measuring 1.2 nm thick according to variable-angle spectroscopic ellipsometry (VASE) measurements. [The gyration diameter of an unperturbed PS arm is ≈6 nm, but the arms in a brush with $\sigma_{PS} \approx 1.13$ will be slightly extended.] Since OTS is hydrophobic (with a water contact angle, WCA, of 105°), PMMA films are first spin-coated onto glass, floated on deionized water (DIW) and then transferred to the OTS SAM, as schematically depicted in Figure 2b. After 15 min of annealing at 180 °C, the PMMA thin film shows signs of dewetting by NG in Figure 2e. This result confirms that, if the carbonyl groups of PMMA are sufficiently distant (1.2 nm in this case) from the hydroxyl groups on silica, hydrogen bonding is thwarted and the thin film destabilizes in similar fashion as PS. If PMMA cannot anchor to the underlying silica substrate in the presence of the OTS monolayer, it is reasonable to expect that other acrylates (such as PEGDMA) would likewise be unable to do so. For comparison, CSMG NP films of comparable thickness have been prepared in an identical fashion as the PMMA films and likewise floated onto the OTS SAM (*cf.* Figure 2c). Surprisingly and unlike the PMMA films, the CSMG NP films are observed to remain stable after 72 h of annealing at 180 °C (*cf.* Figure 2f). This finding unequivocally establishes that the remarkable stability of the organic NP coatings examined here cannot be attributed to physical interactions between the PEGDMA NP core and the silica substrate.

To ascertain if the stability of the 10 nm CSMG NP thin films on the OTS SAM is due to the NP molecular

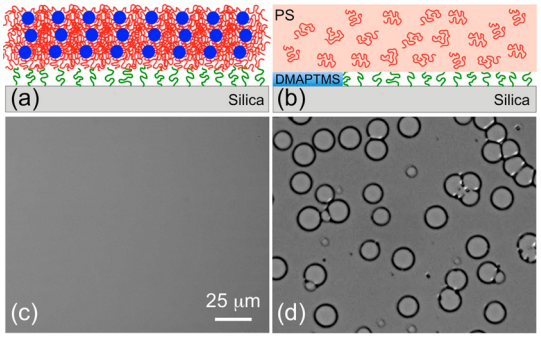

Figure 3. Schematic diagrams of (a) CSMG NP and (b) PS thin films (10 nm) spin-coated on DMAPTMS SAMs measuring 0.8 nm thick. Corresponding optical images of the thin films annealed at 180 °C are displayed for (c) 72 h and (d) 15 s.

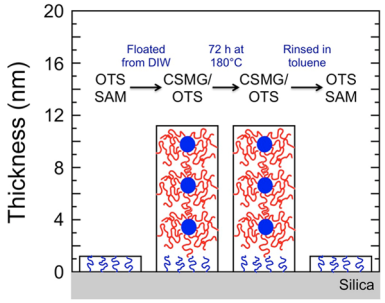

Figure 4. Ellipsometric thickness measurements and associated illustrations of OTS SAMs (thickness: 1.2 nm) with and without a CSMG NP film (thickness: 10 nm). The sequence (from left to right) portrays the SAM, the thin film floated on the SAM, the thin film on the SAM after 72 h at 180 °C, and the remaining SAM after the thin film is subsequently redissolved in toluene.

weight, we have also examined the stability of 10 nm films of the two high-molecular-weight PS grades on OTS SAMs after exposure to the same annealing conditions used to generate Figure 2f. Unlike the stable results observed for analogous PS films spin-coated on silica substrates, the films deposited on OTS substrates appear fully dewetted, as evidenced by the images included in the Supporting Information. For comparison, the stability of 10 nm films of a high-molecular-weight poly(styrene-*ran*-methyl methacrylate) (PS-*ran*-PMMA) copolymer (558 kDa) on silica and OTS substrates has been explored after 72 h at 180 °C and yields similar results as the high-molecular-weight PS homopolymers: the films on silica remain stable, whereas the films on OTS fully dewet. These observations unequivocally indicate that the CSMG NP films possess unique thermal stability attributes. In an effort to destabilize the CSMG NP thin films, the polarity of the silica substrate is modified through the deposition of a *N*,*N*-dimethylaminopropyl trimethoxysilane (DMAPTMS) SAM with a thickness of 0.8 nm according to VASE. Because DMAPTMS is moderately hydrophilic (WCA $\approx$ 60°), thin films measuring 10 nm thick of the CSMG NPs and PS homopolymer (13.5 kDa) can be spin-coated directly from toluene solutions on the SAM, as illustrated in Figure 3, panels a and b, respectively. Optical images of the two systems collected at 180 °C reveal that the NP-based film again remains stable after being annealed for 72 h (Figure 3c), while the PS film starts to dewet after just 15 s (Figure 3d). Taken together, the results presented in Figures 2 and 3 demonstrate that the stability of the CSMG NP films is not sensitive to substrate chemistry/polarity or film thickness over the range of thicknesses examined. With these two effects dismissed, the only reason left to explain the unusual stability of CSMG NP films pertains to impeded molecular mobility. Since the PS arms on the NPs are below $M_{e,PS}$ and since the linear PS homopolymer of comparable molecular weight readily destabilizes under the conditions investigated here, impeded flow in the case of the CSMG NP films does not appear to be a result of chain entanglement as in conventional homopolymer thin films. Rather, we hypothesize that the dense brushes of PS arms on neighboring NPs interpenetrate in all directions to immobilize the NPs and thus maintain the integrity of thin NP films.

Although the OTS SAM employed here appears to be sufficiently thick to minimize, if not eliminate altogether, hydrogen bonding between the CSMG NP film deposited on top and the silica substrate below, the possibility that the CSMG NPs are somehow additionally stabilized by mixing with the OTS molecules cannot be discounted. This situation is particularly important when the film thickness approaches monolayer coverage (according to an independent AFM analysis,[62] a monolayer would measure $\approx$3 nm thick). To ascertain if interlayer mixing occurs, we have floated a NP layer measuring 10 nm thick on top of the OTS SAM, dried the bilayered construct overnight at ambient temperature, annealed the bilayer for 72 h at 180 °C, and finally subjected the system to a toluene rinse. The results of this sequence of events are displayed in Figure 4 and reveal two important outcomes. First, the thicknesses of the two layers (1.2 nm from the OTS monolayer and 10 nm from the CSMG NP film) are additive (to 11.2 nm) after the initial deposition of the top layer, as well as after the extended heat treatment, verifying that they do not mix to a discernible extent. Second, the NPs are not chemically cross-linked since they readily redissolve in toluene, leaving behind only the OTS SAM at its original thickness. These observations are consistent with our proposed hypothesis that the NPs remain stable as thin films due to a physical process involving multidirectional interpenetration of the densely grafted PS arms comprising the shell of the CSMG NPs.

The data shown in Figures 2–4 have been collected from CSMG NP thin films that measure 10 nm thick and thus approximate a trilayer. Recalling from Figure 4 that such films deposited onto SAMs can be redissolved in toluene even after prolonged high-temperature treatment, we now return to explore the dissolution characteristics of a thicker (40 nm) film spin-coated

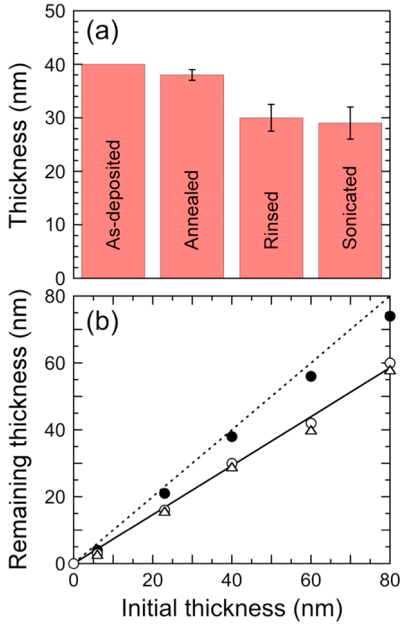

Figure 5. In (a), ellipsometric thickness measurements of a CSMG NP film spin-coated to 40 nm onto Si wafer after different stages (labeled): deposited (at ambient temperature), annealed (for 24 h at 180 °C), rinsed (quiescently in toluene), and sonicated (also in toluene). The error bars represent the standard error in the data. In (b), remaining film thickness as a function of initial CSMG NP film thickness after annealing (●), rinsing (○) and sonication (△). The dashed line corresponds to as-deposited films (where the initial and remaining thicknesses are equal), and the solid line is a linear regression to the data obtained by rinsing. The ratio of their slopes reveals that the annealed film thickness after rinsing is consistently about 73% of the initial thickness.

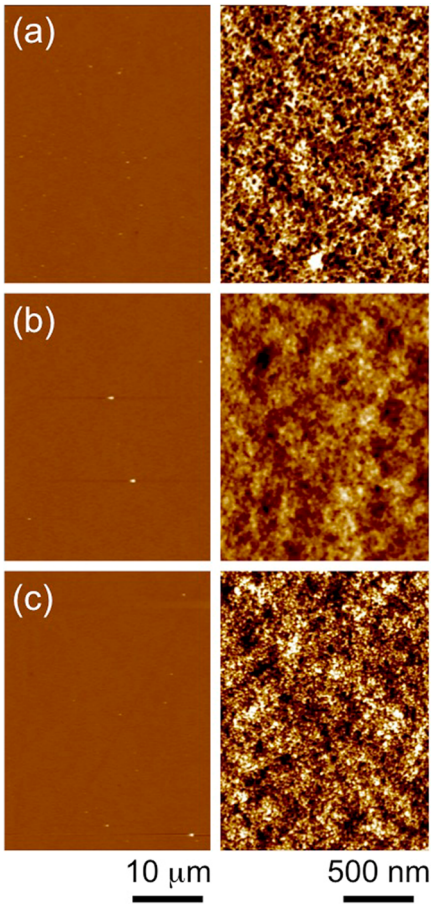

Figure 6. AFM height images acquired from the CSMG NP films discussed in relation to Figure 5a: (a) as-deposited from toluene (thickness: 40 nm), (b) annealed at 180 °C for 24 h (thickness: 38 nm), and (c) rinsed in toluene (thickness: 30 nm). Enlargements (shade-coded as dark at −2.0 nm and light as +2.0 nm) are included in each part to facilitate examination of individual NPs.

directly onto Si wafer. According to the VASE results displayed in Figure 5a, the thickness of the film decreases slightly (to 38 nm) after annealing at 180 °C for 24 h, suggesting that the film densifies as the NPs pack more efficiently. This observation may be related to thermal jamming,[73] a process by which polymer chains surface-grafted to solid inorganic nanoparticles seek to interpenetrate to fill loosely packed interstitial space. [We discount here the likelihood of densification due to solvent evaporation on the basis of toluene diffusion considerations[74,75] through glassy PS films measuring 40 nm in thickness.] Rinsing this annealed film with toluene promotes a further reduction to 30 nm, which—interestingly—corresponds to a loss of the top 8 nm (nearly a trilayer of NPs). This result is likewise attained when the rinsing time (with intermittent agitation) is extended to 24 h, suggesting that the film is remarkably robust and may be an excellent candidate for coating applications. Despite the addition of significant acoustic energy, sonication applied for 2 min during rinsing has little effect on film thickness beyond rinsing alone, whereas sonication conducted for 60 min in toluene removes all but the bottom 5 nm (a little more than an expected monolayer) of the CSMG NP film. One noticeable change in the films after sonication is the introduction of discrete holes, which are discussed in more detail below. [Due to the presence of holes, however, the refractive index of each film must be corrected in the film thickness calculation included in Figure 5. This correction is provided in the Supporting Information.] Similar responses of the NP films to solvent exposure are likewise observed at other film thicknesses, as evidenced by the results presented in Figure 5b. The corresponding surface topologies of the CSMG NP films after deposition, annealing and rinsing in Figure 5a are visible in the AFM height images provided in Figure 6, panels a, b, and c, respectively. While the low-magnification images show little difference, the high-magnification images reveal that the NPs initially form sharply defined features (including individual NPs measuring 15.7 ± 1.4 nm in diameter) that comprise hills and valleys varying from −2 to +2 nm in height (with an rms roughness of 0.94 nm) in Figure 6a. These features are much less pronounced after annealing in Figure 6b (the rms roughness decreases to 0.49 nm), but they are clearly recovered after the toluene rinse in Figure 6c (the rms roughness increases to 0.87 nm). The

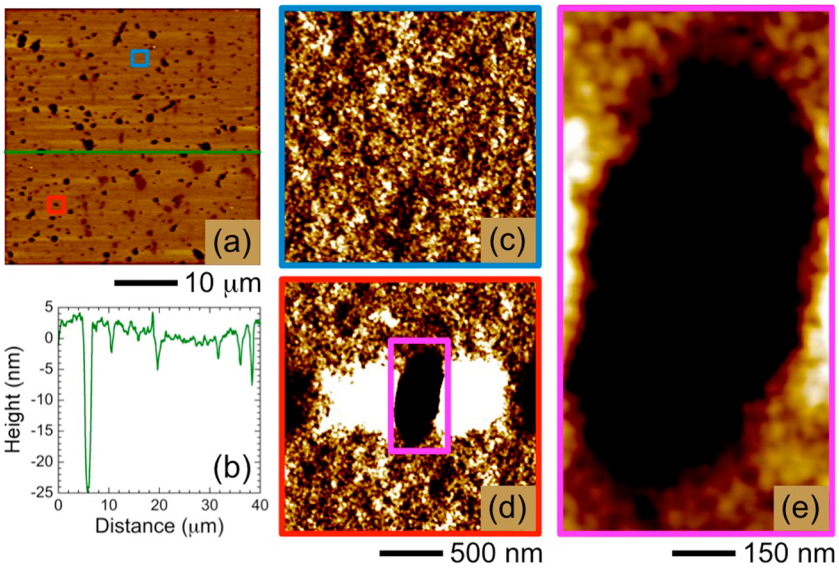

Figure 7. Series of AFM height images and related results collected from the sonicated CSMG NP film introduced in Figure 5a and measuring 29 nm thick after sonication in toluene. An overview image (a) reveals the presence of discrete, rimless holes that are uniformly distributed, and a height trace (b) corresponding to the horizontal line in (a) confirms that such holes extend through the film thickness. The color-coded boxes in (a) identify the spatial positions of the enlargements (shade-coded as dark at −2.0 nm and light as +2.0 nm) provided in (c) and (d). The hole evident in (d) is enlarged further in (e), which is shade-coded from −5.0 to +5.0 nm. Thesholding the image in (e) yields several relevant size and shape metrics: an equivalent area of 0.19 μm^2, a perimeter of 2.35 μm and a circularity of 0.74.

accompanying NP diameters measured from images such as these are 13.6 ± 1.0 and 16.7 ± 1.2 nm, respectively. It must be remembered that, due to the erosion evident in Figure 5a, the film showcased in Figure 6c is thinner than that in Figure 6a,b.

As mentioned earlier, the use of sonication to promote NP dissolution from 40 nm films during solvent rinsing produces discrete holes, which are visible throughout the AFM image displayed in Figure 7a. These holes range from 200 nm to 2 μm in diameter. According to the height profile shown in Figure 7b (which corresponds to the horizontal trace seen in Figure 7a), at least some of the holes are capable of extending all the way through the entire film thickness, which is just under 30 nm according to Figure 5a. Thus, even though the thickness of the film subjected to sonication is not very different from that without sonication, the added energy successfully excavates additional NPs as ill-defined columnar pores extending through the film. Included in Figure 7 are AFM height images acquired from the two identified regions in Figure 7a illustrating no macroscopic features (Figure 7c) and a single hole (Figure 7d). The image presented in Figure 7c closely resembles those obtained from the film after initial deposition (Figure 6a) and solvent rinsing (Figure 6c), and possesses a comparable rms roughness (0.87 nm). In marked contrast, the hole evident in Figure 7d is very different in shape and topology from that generated by classical NG dewetting. [Holes generated by NG are typically circular and possess a well-defined rim.] Close examination of the enlargement of the noncircular, rimless hole in Figure 7e reveals the uneven packing of individual NPs due to erosion along the periphery. Analysis of the corresponding thresholded image, generated with the ImageJ software, yields the size and shape metrics listed in the caption of Figure 7.

Previous studies reported by Tang *et al.*[2] have established that free-floating monolayer films of inorganic NPs measuring a mere 3.4 nm thick can be achieved by carefully exploiting the various forces involved. In the case of organic NPs, an equally important consideration in the production of free-floating homopolymer films is the critical molecular weight of entanglement, since physical chain entanglements are needed to prevent the surface energy of water from breaking the film apart. Since the entanglement molecular weight of linear PS is ≈18 kDa,[66] a stable, free-floating thin film cannot be prepared from PS homopolymer possessing a molecular weight of 13.5 kDa. This is not the case, however, for the CSMG NPs composed of PS arms whose molecular weight is $<M_{e,PS}$. As demonstrated earlier with regard to the preparation of bilayered constructs containing an OTS SAM (*cf.* Figure 2c), a NP film measuring 10 nm thick can be spin-coated onto glass and subsequently floated on DIW, as schematically depicted in Figure 8a. The resultant film, a photograph of which is displayed in Figure 8b, remains stable on the water surface for several days. On a related note, Russell and co-workers[76] have established a procedure by which the mechanical properties of a free-floating linear PS film can be extracted by placing a drop of water on the film and measuring the wrinkles that develop. Application of this procedure to the free-floating CSMG NP film does not, however, yield wrinkles. Instead, positioning a 1 μL DIW

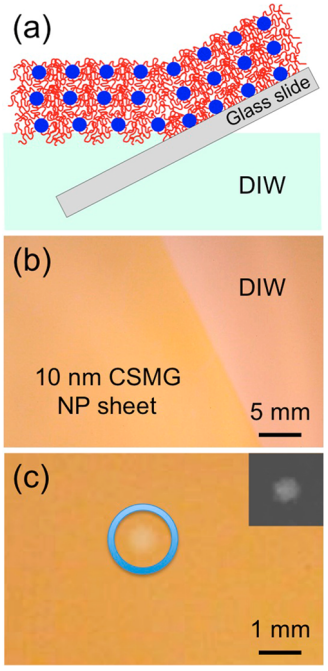

Figure 8. In (a), a cross-sectional illustration of a CSMG NP film (thickness: *ca.* 10 nm) spin-coated onto glass and floated on the surface of DIW. An optical image confirming the stability of such a free-floating NP sheet is provided in (b), whereas the same film after a DIW droplet produces a macroscopic hole is included in (c). The inset in (c) shows the hole in a high-contrast grayscale image.

droplet on the NP film immediately induces a well-defined hole, as evidenced by the photograph included in Figure 8c and the corresponding thresholded image provided in the inset. This result is consistent with the findings associated with Figure 4 and implies that a small number of multilayers may not possess sufficient multidirectional arm penetration to remain stable in the presence of an applied liquid (even if it is not a solvent).

CONCLUSIONS

In this study, we have explored the stabilization attributes of CSMG NP thin films alone and in conjunction with surface-modifying SAMs deposited on silica substrates. Annealing PS homopolymer of approximately the same chain length as the PS arms comprising the shell of the NPs above T_g results in rapid destabilization by NG dewetting. Contrariwise, equivalent CSMG NP films remain stable, displaying no evidence of any dewetting mechanism, for more than 72 h under identical experimental conditions. By introducing a SAM between these films and the silica substrate, we unequivocally establish that hydrogen bonding between the acrylic core of the NPs and silica is not responsible for the observed thin-film stability. Moreover, by examining the thicknesses of NP films and SAMs before and after deposition/dissolution of the films, we discount penetration of the PS arms into the SAM as the origin of such remarkable stability. Relatively thin NP films containing about 3 or less layers and deposited onto SAMs can be fully redissolved even after long-term thermal treatment at 180 °C. Thicker films spin-coated onto Si wafers, however, become only partially soluble under similar conditions, suggesting that the relatively short PS arms interpenetrate from multiple directions within the films to lock-in the positions of the NPs and, in so doing, prevent dissolution even when sonicated. Sonication does introduce holes, which differ substantially in their characteristics from holes generated by NG dewetting, at locations where NPs are vertically excavated from the films. Due to the mechanism by which these NP thin films remain stable, they are able to form free-floating sheets on water at thicknesses of only 10 nm. Since these CSMG NP films do not depend on chain entanglement for their stability, they provide an attractive and viable alternative to organic thin-film coating technologies.

METHODS

Materials. Styrene monomer (S, >99% pure), ethylene glycol dimethacrylate (EGDMA, >98% pure), tetrahydrofuran (THF), hydroquinone (HQ), monomethyl ether hydroquinone (MEHQ), 1-bromoethylbenzene, copper bromide (CuBr), *N*,*N*,*N*′,*N*″,*N*‴-pentamethyldiethylenetriamine (PMDETA), methanol, anhydrous anisole, toluene, and *N*,*N*-dimethylaminopropyl trimethoxysilane (DMAPTMS) were all purchased from Sigma-Aldrich (St. Louis, MO). The S monomer was purified through basic alumina twice, whereas the EGDMA monomer was purified through a sinter bed containing HQ and MEHQ on top of basic alumina. One low-molecular-weight polystyrene (PS) ($\bar{M}_w$ = 13.5 kDa, polydispersity index, PDI, = 1.06) and two high-molecular-weight PS homopolymers ($\bar{M}_w$ = 216 kDa, PDI = 1.06, and $\bar{M}_w$ = 900 kDa, PDI = 1.10) were obtained from Pressure Chemical, Inc. (Pittsburgh, PA), whereas poly(methyl methacrylate) (PMMA) homopolymer ($\bar{M}_w$ = 112 kDa, PDI = 1.09) and a poly(styrene-*ran*-methyl methacrylate) (PS-*ran*-PMMA) copolymer ($\bar{M}_w$ = 558 kDa, PDI = 1.83) were procured from Polymer Source, Inc. (Dorval, Canada). *n*-Octyltrichlorosilane (OTS) was acquired from Gelest, Inc. (Morrisville, PA) and used as-received. Deionized water (resistivity >15 MΩ-cm) was produced using a Millipore water purification system.

Nanoparticle Synthesis and Characterization. The chemical protocol employed for synthesizing poly(ethylene glycol dimethacrylate) core-polystyrene shell (PEGDMA-PS) CSMG NPs by the arm-first approach and ATRP was similar to procedures previously reported by some of us.[77−79] Briefly, a linear PS macroinitiator (*i.e.*, the "arm") was first prepared *via* ATRP of styrene using 1-bromoethylbenzene as the initiator and CuBr/PMDETA as the catalyst complex. To generate CSMG NPs, the PS macroinitiator ($\bar{M}_w$ = 10.7 kDa, PDI = 1.10) was linked together using EGDMA as a cross-linker in the presence of CuBr/PMDETA as the catalyst complex. The crude CSMG was purified *via* fractional precipitation to remove unreacted macroinitiator. Analysis of the isolated PEGDMA-PS CSMG NPs *via* SEC-MALLS yielded $\bar{M}_w$ = 438 kDa and PDI = 1.16, and allowed calculation of the number of arms per NP (32), as well as the molecular weight contribution of the PEGDMA microgel core (96 kDa). Full details describing the synthesis of the CSMG NPs are provided in the Supporting Information.

Film Preparation and Characterization. Thin films of both homopolymers and the NPs were prepared at ambient temperature by spin-coating solutions onto Si wafer with the surface silica layer intact. The linear PS, linear PMMA and CSMG NPs were individually dissolved in toluene at concentrations ranging from

0.2 to 2.0 wt %, and the rotation speed was varied from 800 to 2000 rpm to obtain the desired film thicknesses. Self-assembled monolayers (SAMs) of OTS and DMAPTMS were deposited onto Si wafers according to an established procedure.[80] Briefly, the Si wafers were cleaned *via* ultraviolet/ozone treatment and then rinsed with toluene. After drying the surface with nitrogen, each wafer was suspended upside down on the center of the lid of a Petri dish over a solution of OTS (or DMAPTMS) and mineral oil for 10 min. Film and SAM thicknesses were measured by VASE on a J.A. Woollam Co. instrument. Ellipsometric data were collected at wavelengths ranging from 400 to 1100 nm in 10 nm increments at incidence angles of 70° and 75° relative to the surface normal for the polymer films and SAMs, respectively. Specimen thicknesses were calculated using a Cauchy layer model with the following indices of refraction: 1.45 for the OTS SAM, 1.42 for the DMAPTMS SAM and 1.59 for all other organic compounds.[81] Water contact angle experiments were performed at ambient temperature on a Ramé–Hart Model 100-00 contact-angle goniometer equipped with a CCD camera. Static WCAs were discerned by depositing a 4 μL droplet of DIW at three different positions on a surface and then averaging the measurements. Images of polymer thin films undergoing destabilization by dewetting were acquired with an Olympus BX60 optical microscope equipped with a computer-interfaced CCD camera and operated in reflection mode. Stability studies were performed at 180 °C in a Mettler-Toledo hotstage under a circulating nitrogen gas blanket. The surface topography of NP thin films was examined in air with an Asylum Research AFM instrument operated in the alternating-current tapping mode.

Conflict of Interest: The authors declare no competing financial interest.

Acknowledgment. This study was supported at North Carolina State University by the National Science Foundation and the Office of Naval Research (Grant No. N000141210642). Funding by the Australian Research Council was provided through a Discovery Project Grant (DP0986271).

Supporting Information Available: The Supporting Information provides additional information regarding the synthesis of the CSMG NPs, a detailed description of the ellipsometric analysis, and stability results obtained from high-molecular-weight homo/copolymer thin films deposited on different substrates for further comparison with CSMG NP thin films. The Supporting Information is available free of charge on the ACS Publications website at DOI: 10.1021/acsnano.5b00237.

REFERENCES AND NOTES

1. Glotzer, S. C.; Solomon, M. J.; Kotov, N. A. Self-Assembly: From Nanoscale to Microscale Colloids. *AIChE J.* **2004**, *50*, 2978–2985.
2. Tang, Z.; Zhang, Z.; Wang, Y.; Glotzer, S. C.; Kotov, N. A. Self-Assembly of CdTe Nanocrystals into Free-Floating Sheets. *Science* **2006**, *314*, 274–278.
3. Zhang, Z. L.; Tang, Z. Y.; Kotov, N. A.; Glotzer, S. C. Simulations and Analysis of Self-Assembly of CdTe Nanoparticles into Wires and Sheets. *Nano Lett.* **2007**, *7*, 1670–1675.
4. Srivastava, S.; Santos, A.; Critchley, K.; Kim, K. S.; Podsiadlo, P.; Sun, K.; Lee, J.; Xu, C. L.; Lilly, G. D.; Glotzer, S. C.; et al. Light-Controlled Self-Assembly of Semiconductor Nanoparticles into Twisted Ribbons. *Science* **2010**, *327*, 1355–1359.
5. Xia, Y. S.; Nguyen, T. D.; Yang, M.; Lee, B.; Santos, A.; Podsiadlo, P.; Tang, Z. Y.; Glotzer, S. C.; Kotov, N. A. Self-assembly of Self-Limiting Monodisperse Supraparticles from Polydisperse Nanoparticles. *Nat. Nanotechnol.* **2011**, *6*, 580–587.
6. Schmid, G. *Nanoparticles: From Theory to Application*. Wiley-VCH: Weinheim, 2004.
7. Vauthier, C.; Bouchemal, K. Methods for the Preparation and Manufacture of Polymeric Nanoparticles. *Pharm. Res.* **2009**, *26*, 1025–1058.
8. Tuncel, D.; Demir, H. V. Conjugated Polymer Nanoparticles. *Nanoscale* **2010**, *2*, 484–494.
9. Howes, P.; Green, M.; Bowers, A.; Parker, D.; Varma, G.; Kallumadil, M.; Hughes, M.; Warley, A.; Brain, A.; Botnar, R. Magnetic Conjugated Polymer Nanoparticles as Bimodal Imaging Agents. *J. Am. Chem. Soc.* **2010**, *132*, 9833–9842.
10. Chhour, P.; Gallo, N.; Cheheltani, R.; Williams, D.; Al-Zaki, A.; Paik, T.; Nichol, J. L.; Tian, Z.; Naha, P. C.; Witschey, W. R.; et al. Nanodisco Balls: Control over Surface versus Core Loading of Diagnostically Active Nanocrystals into Polymer Nanoparticles. *ACS Nano* **2014**, *8*, 9143–9153.
11. Perkin, K. K.; Turner, J. L.; Wooley, K. L.; Mann, S. Fabrication of Hybrid Nanocapsules by Calcium Phosphate Mineralization of Shell Cross-Linked Polymer Micelles and Nanocages. *Nano Lett.* **2005**, *5*, 1457–1461.
12. Hu, S.-H.; Chen, S.-Y.; Gao, X. Multifunctional Nanocapsules for Simultaneous Encapsulation of Hydrophilic and Hydrophobic Compounds and On-Demand Release. *ACS Nano* **2012**, *6*, 2558–2565.
13. Wohnhaas, C.; Mailaender, V.; Dröge, M.; Filatov, M. A.; Busko, D.; Avlasevich, Y.; Baluschev, S.; Miteva, T.; Landfester, K.; Turshatov, A. Triplet-Triplet Annihilation Upconversion Based Nanocapsules for Bioimaging under Excitation by Red and Deep-Red Light. *Macromol. Biosci.* **2013**, *13*, 1422–1430.
14. Howes, P. D.; Chandrawati, R.; Stevens, M. M. Colloidal Nanoparticles as Advanced Biological Sensors. *Science* **2014**, *346*, 1247390.
15. Bai, P.; Zhu, G.; Liu, Y.; Chen, J.; Jing, Q.; Yang, W.; Ma, J.; Zhang, G.; Wang, Z. L. Cylindrical Rotating Triboelectric Nanogenerator. *ACS Nano* **2013**, *7*, 6361–6366.
16. Tuncel, D.; Demir, H. V. Conjugated Polymer Nanoparticles. *Nanoscale* **2010**, *2*, 484–494.
17. Liechty, W. B.; Peppas, N. A. Expert Opinion: Responsive Polymer Nanoparticles in Cancer Therapy. *Eur. J. Pharm. Biopharm.* **2012**, *80*, 241–246.
18. Wu, C.; Chiu, D. T. Highly Fluorescent Semiconducting Polymer Dots for Biology and Medicine. *Angew. Chem., Int. Ed.* **2013**, *52*, 3086–3109.
19. Tan, F.; Sun, D.; Gao, J.; Zhao, Q.; Wang, X.; Teng, F.; Quan, X.; Chen, J. Preparation of Molecularly Imprinted Polymer Nanoparticles for Selective Removal of Fluoroquinolone Antibiotics in Aqueous Solution. *J. Hazard. Mater.* **2013**, *244–245*, 750–757.
20. Kim, J. In *Advances in Nanotechnology and the Environment*.; Kim, J., Ed.; Pan Stanford: Singapore, 2011; Chapter 3, pp 45–77.
21. Vanderhoff, J. W.; El-Aasser, M. S.; Ugelstad, J. Polymer Emulsification Process. U.S. Patent 4,177,177, Dec 4, 1979.
22. Zambaux, M. F.; Bonneaux, F.; Gref, R.; Maincent, P.; Dellacherie, E.; Alonso, M. J.; Labrude, P.; Vigneron, C. Influence of Experimental Parameters on the Characteristics of Poly(lactic acid) Nanoparticles Prepared by a Double Emulsion Method. *J. Controlled Release* **1998**, *50*, 31–40.
23. Bindschaedler, C.; Gurny, R.; Doelker, E. Process for Preparing a Powder of Water-Insoluble Polymer Which Can Be Redispersed in a Liquid Phase, the Resulting Powder and Utilization Thereof. U.S. Patent 4,968,350, Nov 6, 1990.
24. Fessi, H.; Puisieux, F.; Devissaguet, J. P.; Ammoury, N.; Benita, S. Nanocapsule Formation by Interfacial Polymer Deposition Following Solvent Displacement. *Int. J. Pharm.* **1989**, *55*, R1–R4.
25. Jeong, Y. I.; Cho, C. S.; Kim, S. H.; Ko, K. S.; Kim, S. I.; Shim, Y. H.; Nah, J. W. Preparation of Poly(DL-lactide-*co*-glycolide) Nanoparticles without Surfactant. *J. Appl. Polym. Sci.* **2001**, *80*, 2228–2236.
26. Jung, J.; Perrut, M. Particle Design Using Supercritical Fluids: Literature and Patent Survey. *J. Supercrit. Fluids* **2001**, *20*, 179–219.
27. Asua, J. M. Emulsion Polymerization: from Fundamental Mechanisms to Process Developments. *J. Polym. Sci., Part A: Polym. Chem.* **2004**, *42*, 1025–1041.
28. Ramirez, A. G.; Lopez, R. G.; Tauer, K. Studies on Semibatch Microemulsion Polymerization of Butyl Acrylate: Influence

of the Potassium Peroxodisulfate Concentration. *Macromolecules* **2004**, *37*, 2738–2747.
29. Ham, H. T.; Choi, Y. S.; Chee, M. G.; Chung, I. J. Singlewall Carbon nanotubes Covered with Polystyrene Nanoparticles by *In-Situ* Miniemulsion Polymerization. *J. Polym. Sci., Part A: Polym. Chem.* **2006**, *44*, 573–584.
30. Scott, C.; Wu, D.; Ho, C. C.; Co, C. C. Liquid-Core Capsules *via* Interfacial Polymerization: a Free-Radical Analogy of the Nylon Rope Trick. *J. Am. Chem. Soc.* **2005**, *127*, 4160–4161.
31. Matyjaszewski, K.; Xia, J. Atom Transfer Radical Polymerization. *Chem. Rev.* **2001**, *101*, 2921–2990.
32. Zetterlund, P. B.; Kagawa, Y.; Okubo, M. Controlled/Living Radical Polymerization in Dispersed Systems. *Chem. Rev.* **2008**, *108*, 3747–3794.
33. Bansal, A.; Yang, H.; Li, C.; Cho, K.; Benicewicz, B. C.; Kumar, S. K.; Schadler, L. S. Quantitative Equivalence between Polymer Nanocomposites and Thin Polymer Films. *Nat. Mater.* **2005**, *4*, 693–698.
34. Akcora, P.; Liu, H.; Kumar, S. K.; Moll, J.; Li, Y.; Benicewicz, B. C.; Schadler, L. S.; Acehan, D.; Panagiotopoulos, A. Z.; Pryamitsyn, V.; et al. Anisotropic Self-assembly of Spherical Polymer-Grafted Nanoparticles. *Nat. Mater.* **2009**, *8*, 354–359.
35. Harton, S. E.; Kumar, S. K.; Yang, H.; Koga, T.; Hicks, K.; Lee, H. K.; Mijovic, J.; Liu, M.; Vallery, R. S.; Gidley, D. W. Immobilized Polymer Layers on Spherical Nanoparticles. *Macromolecules* **2010**, *43*, 3415–3421.
36. Kalathi, J. T.; Grest, G. S.; Kumar, S. K. Universal Viscosity Behavior of Polymer Nanocomposites. *Phys. Rev. Lett.* **2012**, *109*, 198301.
37. Gan, D. J.; Lyon, L. A. Tunable Swelling Kinetics in Core-Shell Hydrogel Nanoparticles. *J. Am. Chem. Soc.* **2001**, *123*, 7511–7517.
38. Duval, J. F. L.; Ohshima, H. Electrophoresis of Diffuse Soft Particles. *Langmuir* **2006**, *22*, 3533–3546.
39. Richtering, W. Responsive Emulsions Stabilized by Stimuli-Sensitive Microgels: Emulsions with Special Non-Pickering Properties. *Langmuir* **2012**, *28*, 17218–17229.
40. Liu, Y. Y.; Liu, X. Y.; Yang, J. M.; Lin, D. L.; Chen, X.; Zha, L. S. Investigation of Ag Nanoparticles Loading Temperature Responsive Hybrid Microgels and Their Temperature Controlled Catalytic Activity. *Colloids Surf., A* **2012**, *393*, 105–110.
41. Welsch, N.; Becker, A. L.; Dzubiella, J.; Ballauff, M. Core-Shell Microgels as "Smart" Carriers for Enzymes. *Soft Matter* **2012**, *8*, 1428–1436.
42. Silan, C.; Akcali, A.; Otkun, M. T.; Ozbey, N.; Butun, S.; Ozay, O.; Sahiner, N. Novel Hydrogel Particles and Their IPN Films as Drug Delivery Systems with Antibacterial Properties. *Colloids Surf., B* **2012**, *89*, 248–253.
43. Uppapalli, S.; Zhao, H. Polarization of a Diffuse Soft Particle Subjected to an Alternating Current Field. *Langmuir* **2012**, *28*, 11164–11172.
44. Wiese, S.; Spiess, A. C.; Richtering, W. Microgel-Stabilized Smart Emulsions for Biocatalysis. *Angew. Chem., Int. Ed.* **2013**, *52*, 576–579.
45. Blencowe, A.; Tan, J. F.; Goh, T. K.; Qiao, G. G. Core Cross-Linked Star Polymers *via* Controlled Radical Polymerisation. *Polymer* **2009**, *50*, 5–32.
46. Mei, Y.; Lu, Y.; Polzer, F.; Ballauff, M.; Drechsler, M. Catalytic Activity of Palladium Nanoparticles Encapsulated in Spherical Polyelectrolyte Brushes and Core-Shell Microgels. *Chem. Mater.* **2007**, *19*, 1062–1069.
47. Ballauff, M.; Lu, Y. Smart" Nanoparticles: Preparation, Characterization and Applications. *Polymer* **2007**, *48*, 1815–1823.
48. Thurmond, K. B.; Kowalewski, T.; Wooley, K. L. Shell Cross-Linked Knedels: A Synthetic Study of the Factors Affecting the Dimensions and Properties of Amphiphilic Core-Shell Nanospheres. *J. Am. Chem. Soc.* **1997**, *119*, 6656–6665.
49. Huang, H.; Remsen, E. E.; Wooley, K. L. Amphiphilic Core-shell Nanospheres Obtained by Intramicellar Shell Cross-linking of Polymer Micelles with Poly(ethylene oxide) Linkers. *Chem. Commun.* **1998**, 1415–1416.
50. Wooley, K. L. Shell Crosslinked Polymer Assemblies: Nanoscale Constructs Inspired from Biological Systems. *J. Polym. Sci., Part A: Polym. Chem.* **2000**, *38*, 1397–1407.
51. Joralemon, M. J.; O'Reilly, R. K.; Hawker, C. J.; Wooley, K. L. Shell Click-Crosslinked (SCC) Nanoparticles: A New Methodology for Synthesis and Orthogonal Functionalization. *J. Am. Chem. Soc.* **2005**, *127*, 16892–16899.
52. Gao, H.; Matyjaszewski, K. Synthesis of Functional Polymers with Controlled Architecture by CRP of Monomers in the Presence of Cross-linkers: From Stars to Gels. *Prog. Polym. Sci.* **2009**, *34*, 317–350.
53. Wei, B.; Gurr, P. A.; Gozen, A. O.; Blencowe, A.; Solomon, D. H.; Qiao, G. G.; Spontak, R. J.; Genzer, J. Autophobicity-Driven Surface Segregation and Patterning of Core-Shell Microgel Nanoparticles. *Nano Lett.* **2008**, *8*, 3010–3016.
54. Barnes, K. A.; Karim, A.; Douglas, J. F.; Nakatani, A. I.; Gruell, H.; Amis, E. J. Suppression of Dewetting in Nanoparticle-filled Polymer Films. *Macromolecules* **2000**, *33*, 4177–4185.
55. Barnes, K. A.; Douglas, J. F.; Liu, D. W.; Karim, A. Influence of Nanoparticles and Polymer Branching on the Dewetting of Polymer Films. *Adv. Colloid Interface Sci.* **2001**, *94*, 83–104.
56. Roy, S.; Bandyopadhyay, D.; Karim, A.; Mukherjee, R. Interplay of Substrate Surface Energy and Nanoparticle Concentration in Suppressing Polymer Thin Film Dewetting. *Macromolecules* **2015**, *48*, 373–382.
57. Mukherjee, R.; Das, S.; Sharma, S. K.; Raychaudhuri, A. K.; Sharma, A. Stability and Dewetting of Metal Nanoparticle Filled Thin Polymer Films: Control of Instability Length Scale and Dynamics. *ACS Nano* **2010**, *4*, 3709–3724.
58. Amarandei, G.; Clancy, I.; O'Dwyer, C.; Arshak, A.; Corcoran, D. Stability of Ultrathin Nanocomposite Polymer Films Controlled by the Embedding of Gold Nanoparticles. *ACS Appl. Mater. Interfaces* **2014**, *6*, 20758–20767.
59. Krishnan, R. S.; Mackay, M. E.; Hawker, C. J.; Van Horn, B. Influence of Molecular Architecture on the Dewetting of Thin Polystyrene Films. *Langmuir* **2005**, *21*, 5770–5776.
60. Mackay, M. E.; Hong, Y.; Jeong, M.; Hong, S.; Russell, T. P.; Hawker, C. J.; Vestberg, R.; Douglas, J. F. Influence of Dendrimer Additives on the Dewetting of Thin Polystyrene Films. *Langmuir* **2002**, *18*, 1877–1882.
61. Xu, L.; Yu, X.; Shi, T.; An, L. Dewetting of Linear Polymer/Star Polymer Blend Film. *Macromolecules* **2008**, *41*, 21–24.
62. Cai, X.-J. Ph.D. Dissertation, North Carolina State University: Raleigh, NC, 2013.
63. Terashima, T.; Motokawa, R.; Koizumi, S.; Sawamoto, M.; Kamigaito, M.; Ando, T.; Hashimoto, T. *In Situ* and Time-Resolved Small-Angle Neutron Scattering Observation of Star Polymer Formation *via* Arm-Linking Reaction in Ruthenium-Catalyzed Living Radical Polymerization. *Macromolecules* **2010**, *43*, 8218–8232.
64. Sheiko, S. S.; Sumerlin, B. S.; Matyjaszewski, K. Cylindrical Molecular Brushes: Synthesis, Characterization, and Properties. *Prog. Polym. Sci.* **2008**, *33*, 759–785.
65. Reiter, G. Dewetting of Thin Polymer Films. *Phys. Rev. Lett.* **1992**, *68*, 75–78.
66. Ferry, J. D. *Viscoelastic Properties of Polymers*, 3rd ed.; Wiley-VCH: Weinheim, 1980.
67. Reiter, G. Dewetting of Highly Elastic Thin Polymer Films. *Phys. Rev. Lett.* **2001**, *87*, 186101.
68. Brochart-Wyart, F.; Dalliant, J. Drying of Solids Wetted by Thin Liquid Films. *Can. J. Phys.* **1990**, *68*, 1084–1088.
69. Xie, R.; Karim, A.; Douglas, J. F.; Han, C. C.; Weiss, R. A. Spinodal Dewetting of Thin Polymer Films. *Phys. Rev. Lett.* **1998**, *81*, 1251–1254.
70. Cheng, J. Y.; Ross, C. A.; Smith, H. I.; Thomas, E. L. Templated Self-Assembly of Block Copolymers: Top-Down Helps Bottom-Up. *Adv. Mater.* **2006**, *18*, 2505–2521.
71. Cai, X.-J.; Genzer, J.; Spontak, R. J. Evolution of Homopolymer Thin-Film Instability on Surface-Anchored Diblock Copolymers Varying in Composition. *Langmuir* **2014**, *30*, 11689–11695.
72. Landry, C. J. T.; Coltrain, B. K.; Wesson, J. A.; Zumbulyadis, N.; Lippert, J. L. *In Situ* Polymerization of Tetraethoxysilane in Polymers: Chemical Nature of the Interactions. *Polymer* **1992**, *33*, 1496–1506.

73. Agarwal, P.; Srivastava, S.; Archer, L. A. Thermal Jamming of a Colloidal Glass. *Phys. Rev. Lett.* **2011**, *107*, 268302.
74. Pickup, S.; Blum, F. D. Self-Diffusion of Toluene in Polystyrene Solutions. *Macromolecules* **1989**, *22*, 3961–3968.
75. Zielinski, J. M.; Duda, J. L. Predicting Polymer/Solvent Diffusion Coefficients Using Free-Volume Theory. *AIChE J.* **1992**, *38*, 405–415.
76. Huang, J. S.; Juszkiewicz, M.; de Jeu, M. H.; Cerda, E.; Emrick, T.; Menon, N.; Russell, T. P. Capillary Wrinkling of Floating Thin Polymer Films. *Science* **2007**, *317*, 650–653.
77. Goh, T. K.; Coventry, K. D.; Blencowe, A.; Qiao, G. G. Rheology of Core Cross-Linked Star Polymers. *Polymer* **2008**, *49*, 5095–5104.
78. Spiniello, M.; Blencowe, A.; Qiao, G. G. Synthesis and Characterization of Fluorescently Labeled Core Cross-Linked Star Polymers. *J. Polym. Sci., Part A: Polym. Chem.* **2008**, *46*, 2422–2432.
79. Blencowe, A.; Goh, T. K.; Best, S. P.; Qiao, G. G. Synthesis of Buckminsterfullerene C_{60} Functionalised Core Cross-Linked Star Polymers. *Polymer* **2008**, *49*, 825–830.
80. Sagiv, J. Organized Monolayers by Adsorption, I. Formation and Structure of Oleophobic Mixed Monolayers on Solid Surfaces. *J. Am. Chem. Soc.* **1980**, *102*, 92–98.
81. Brandrup, J.; Immergut, E. H.; Grulke, E. A. *Polymer Handbook*; Wiley-VCH: Weinheim, 2004.